Hot electron production at shock-ignition-relevant conditions characterized by high-resolution x-ray spectroscopy & imaging

O. RENNER[1], M. ŠMÍD[1,2]

[1]*Institute of Physics, Academy of Sciences CR, Prague, Czech Republic*
[2]*Czech Technical University in Prague, FNSPE, Prague, Czech Republic*

Further collaboration:
University of Bordeaux, CNRS, CEA, CELIA, UMR 5107, Talence, France
LULI, École Polytechnique, & Sorbonne Universités, UPMC, Paris,France
Institute of Plasma Physics and Laser Microfusion, Warsaw, Poland

Joint ICTP-IAEA Advanced School and Workshop on Modern Methods in Plasma Spectroscopy 16-27 March 2015, Miramare- Trieste, Italy

Outline of the Talk

Selected aspects of wavelength-dispersive x-ray spectroscopy
- Diagnostic potential of high-resolution x-ray spectra
- Spectroscopic principles and experimental limits of Bragg-crystal x-ray spectroscopy

Sample application:
- Hot electron production at SI-relevant conditions characterized by combined methods of x-ray spectroscopy and quasi-monochromatic imaging

Acknowledgments

This research was supported by Academy of Sciences project M100101208 and MSMT ELI Project No. CZ.1.05/1.1.00/02.0061

Characteristic Features of Highly Resolved K-Shell Spectra

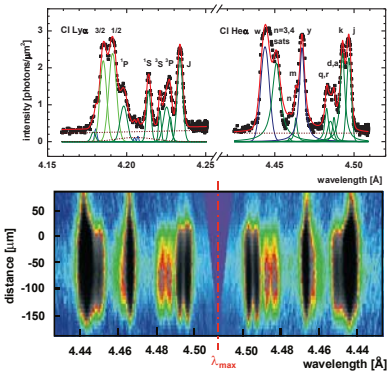

Jungwirth K. et al, Phys. Plasmas ***8*** *(2001) 2495*
Limpouch J. et al, J. Phys. Conf. Ser. ***112*** *(2008) 042056*

Energy deposition in underdense foams
Cl-doped TMPTA
$C_{15}H_{20}O_6$
10 mg/cm³, 20% Cl
PALS laser
(200 J, 0.44 μm, 0.25 ns)
volumetric plasma
$n_e \sim 2\text{-}3\times10^{21}$ cm^{-3}
$T_e \sim 600$ eV
Cl Heα source radiance
~200 ph/(μm² mrad²)
full emission
2.6×10^{13} photons/4π
laser light conversion to Heα group 0.02%

Diagnostic Potential of High-Resolution X-ray Spectra

Routine plasma diagnosis

based on spectral lines identification, their ratios and broadening
Griem H.R., Principles of Plasma Spectroscopy, Cambridge 1997
interpretation primarily in terms of macroscopic plasma parameters (temperature, density, degree of ionization, ion velocity) & gradients
Salzmann D., Atomic Physics in Hot Plasmas, Oxford University Press, 1988
benefiting from available and generally accepted diagnostic codes
FLYCHK: Chung H.K. et al, HEDP ***1*** *(2005) 3;*
PrismSPECT: J.J. MacFarlane et al, HEDP ***3*** *(2007) 181*

Advanced diagnostics

based on specialized codes and detailed interpretation of spectral line profiles, their satellite structure, shifts and radiative transfer effects
Oks E., Plasma Spectroscopy, Springer, Berlin 1995; Rosmej F., JPB ***30*** *(1997) L819*
Renner O. et al, AIP Conf. Proc. ***1058*** *(2008) 341; Scott H.A., JQSRT* ***71*** *(2001) 689*
provides information on diverse processes occurring in plasmas (non-Maxwellian plasma, charge exchange, el. & mg. field effects, ...)
Rosmej F., Highly Charged Ion Spectroscopic Research, p, 267, Taylor and Francis, 2012

Goals and Prerequisites of X-ray Plasma Spectroscopy

Goals

- Exploration of ultradense plasma formations where x rays offer the most efficient and sometimes the only vehicle capable of providing detailed information required
- Diagnosis of environmental conditions in hot dense matter via passive (self-emission) or active (probing the plasma by external x-ray sources) methods
- Investigation of phenomena accompanying creation and evolution of strongly coupled and correlated plasmas

Prerequisites

- Understanding the connection between the measured radiative properties and underlying processes in extreme-state matter
- Application of well tested advanced x-ray instrumentation suitable for obtaining high quality spectroscopic data

Basic & Advanced Principles of X-ray Crystal Spectroscopy

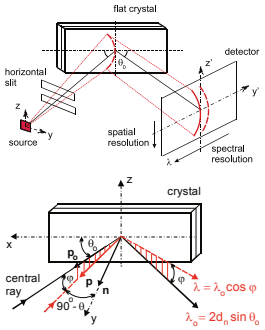

Bragg law: $n\lambda = 2d_n \sin\theta_0$
dispersion: $d\theta/d\lambda = \tan\theta/\lambda$
factors influencing resolution:
source size
reflection curve FWHM
detector pixel size

vertical geometry: $\lambda = \lambda_0 \cos\varphi$
dispersion: $d\varphi/d\lambda = -1/(\lambda \tan\varphi)$
two symmetric spectra
extremely high dispersion
low apparatus smearing
low λ range coverage

Design of advanced experiments: Rigorous description of x-ray diffraction
High collection efficiency → focusing schemes
Combined spectral, spatial & time resolution
Boiko V.A. et al, JQSRT ***19*** *(1978) 11; Hauer A., Laser Part. Beams* ***9*** *(1991) 3*

Application of 1D or 2D Bent Crystals

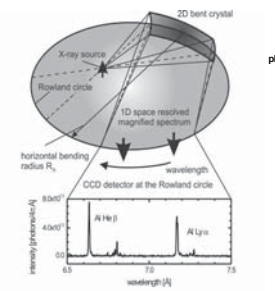

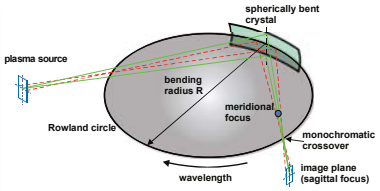

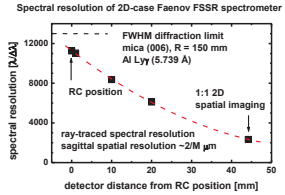

mirror equation: $1/p + 1/q = 1/f_{h,v}$
focal lengths: $f_h = (R_h \sin\theta)/2$
$f_v = R_v/(2 \sin\theta)$
magnification: $M = q/p$

Renner O. et al, Laser Part. Beams ***22*** *(2004) 25; Faenov A.Ya. et al, Phys. Scr.* ***50*** *(1994) 333*

Frequently Used Bent Bragg-Crystal Configurations

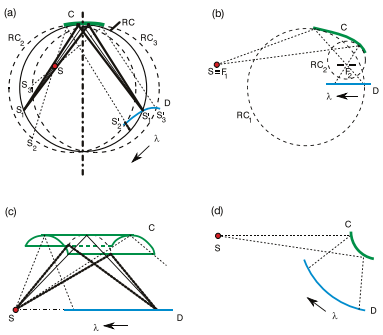

Application criteria:
resolution:
spectral
spatial
temporal (compatibility)
luminosity:
toroidally bent crystals
Von Hamos scheme
wavelength coverage:
convex crystals
crossover existence:
elliptically bent crystals
crystal quality
availability, stability etc.

Design of experiments and reconstruction of the measured data assisted by ray-tracing codes
e.g., Shadow: M.S. del Rio et al., J. Synch. Rad. **18** (2011) 708, *http://ftp.esrf.eu/pub/scisoft/shadow3/*
X-ray for Windows: Podorov S.G. et al, J. Phys. D ***34*** *(2001) 2363*

Spectra Distortion: Crystal Bending and Absorption Edges

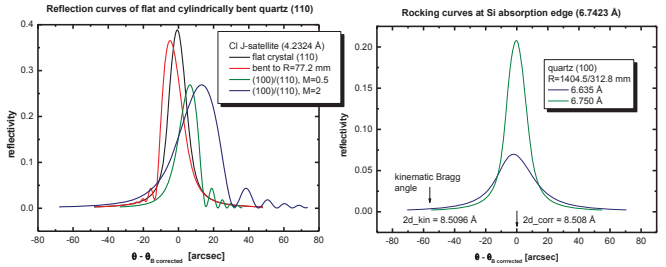

Change of rocking curves due to crystal bending (Cl Lyα emission from foam target) and proximity of absorption edges (Al Heβ group) may result in a non-negligible distortion of the measured spectra. *Hölzer G. et al, Cryst. Res. Technol.* ***33*** *(1998) 555*
Limpouch J. et al, J. Phys. Conf. Ser. ***112*** *(2008) 042056; Woolsey N.C. et al, JQSRT* ***99*** *(2006) 680*

Wavelength Coverage vs. Collection Efficiency

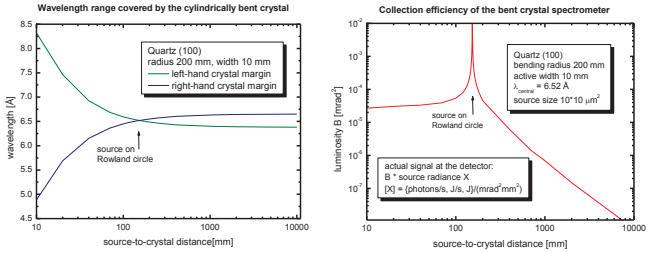

Ray-traced using the code X-ray for Windows: Podorov S.G. et al, J. Phys. D ***34*** *(2001) 2363*

Testing the Crystal Performance

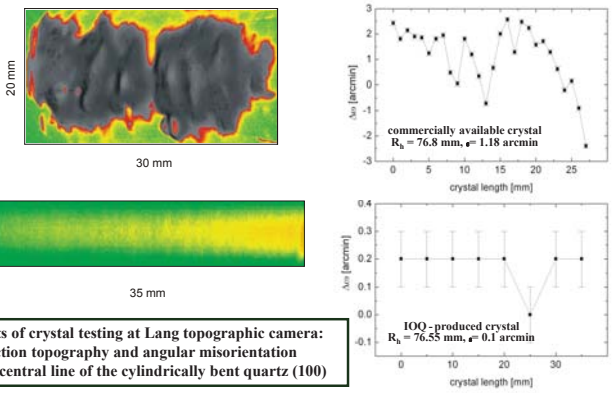

Results of crystal testing at Lang topographic camera: projection topography and angular misorientation along central line of the cylindrically bent quartz (100)

O. Renner, S.G. Podorov, O. Wehrhan, and E. Förster, RSI ***75*** *(2004) 4569*

Comment on Interpretation of Complex Spectra

General approach to evaluation of measured data
A. Raw data reconstruction using transmission function of (absolutely) calibrated apparatus
B. Extraction of the diagnostic features from complex spectra
C. Data interpretation relating observation to underlying processes (via synthesized spectra)

Application of tailored Genetic Algorithm codes (complemented with theoretical input)
parallel global search based on a simulated natural selection *Goldberg D.E., 1989*
problem-oriented approach *Golovkin I.E. et al, JQSRT* ***75*** *(2002) 625*

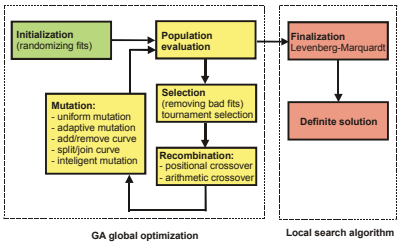

Prague GA code GASPED
- pseudo-Voigt line profiles
- genome size: 26-62 parameters
- population: 250 - 500 genomes
- 8 operators tailored to a problem of spectral decomposition
- number of generations ~ 1000
- final fit refined by L-M method

Adámek P. et al, LPB ***24*** *(2006) 511*

Sample Genetic Algorithm Decomposition of Ti Heβ Group

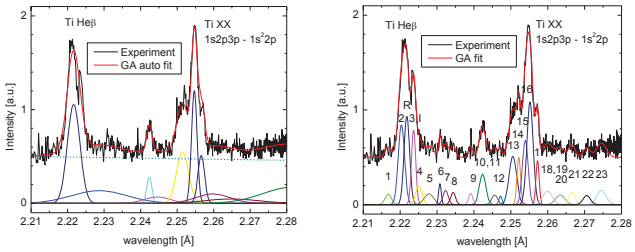

Experiment: LULI 2000nano, 2ω (527 nm), energy 130 J, 0.25 ns,
target Ti foil, thickness 1 μm + tamper teflon 2 μm
VJS quartz (202), 2d=3.3432 Å, R=76.60 mm, Kodak CX film
Ti Heβ group emission analyzed 40 μm below original Ti surface
Automated Fit: setting: 15 pseudo-Voigt profiles, result: 10 lines + bckg
Advanced Fit: theoretical input MARIA code *Rosmej F., JPB* ***30*** *(1997) L819*
setting: 22 lines, population 100, 1500 generations, L-M fit
Diagnostically important group: 2.22-2.23 Å density, 2.25-2.26 Å temperature

K-Shell X-Ray Diagnosis of Hot Electron Generation in Laser-Irradiated Cu Foils

Motivation for studying hot electron (HE) generation & propagation
a key issue for applications of ultraintense lasers:
matter at extreme conditions (EoS, astrophysics, opacities, electron transport dynamics, self-generated elmg fields)
ultrashort intense radiation & particle sources
Suprathermal electron impact on alternate ICF scenarios (direct & indirect, fast & shock ignition schemes):
+ energy transport, ablation pressure enhancement in SI
- preheating of pre-compressed targets
Principal experimental information is collected via x-ray diagnosis:
insight into hot electrons generation & transport in targets
Development of reliable diagnostic methods is a very actual task
Köster P et al, PPCF **51** (2009) 014007*; Nilson PM et al, PoP* ***18*** *(2011) 042702; Galtier E et al, JPB* ***45*** *(2012) 205701; Guskov SYu et al, LPB* ***32*** *(2014) 177*

Diagnostic Setup Applied in PALS Experiments

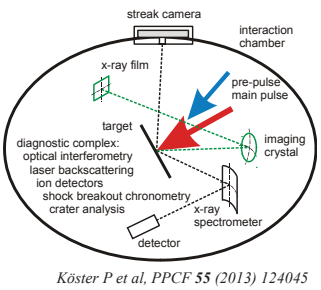

Köster P et al, PPCF ***55*** *(2013) 124045*

Prague iodine laser system
Gaussian 1ω beam
(~440 J, 1.315 μm, 0.3 ns)
focused to ≤ 2×10^{16} W/cm²
[+prepulse 60 J, 8×10^{13} W/cm²]
3ω beam (170 J, 0.44 μm, 0.25 ns)
≤ 9×10^{15} W/cm²
Jungwirth K et al, PoP ***8*** *(2001) 2495*

Plasma production
1.5/10-μm-thick foils, massive Cu
normal laser incidence

Principal X-ray diagnostics used
plasma evolution monitored by pinhole + X-ray streak camera
2D monochromatic imaging, quartz (422), R=380 mm, M=1.73, θ_B=88.15°, ψ~45°
1D resolving x-ray spectrometer, spherical quartz (223), R=150, M=0.51, ψ=10°
high dispersion spectrometer, cylindrical quartz (400), R=76.6, M=1, ψ=0.8±0.8°
signal detected on film Kodak AA400, scanned with resolution 5.3 μm

2D Quasi-Monochromatic Cu K-shell Imaging

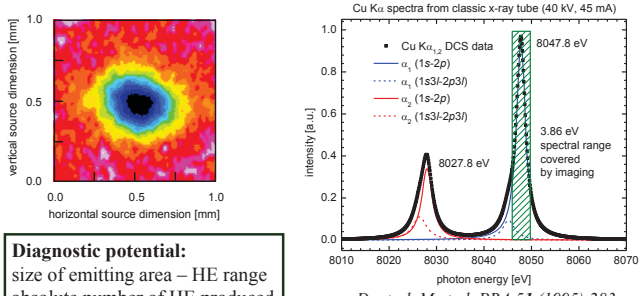

Diagnostic potential:
size of emitting area – HE range
absolute number of HE produced

Deutsch M et al, PRA ***51*** *(1995) 283*

HE-induced collisional processes:
hole creation in inner shells results in K-shell fluorescence; Cu Kα: $2p \rightarrow 1s$
High dispersion imaging: range covered by crystal 3.86 eV
cf. FWHM of cold material Cu $K\alpha_1$ (2.29 eV) – corrections via spectroscopy

Cu K-shell Emission vs. Iλ² Coupling Parameter

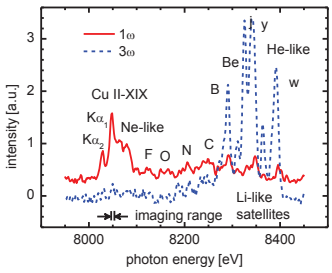

Comparison of 1ω and 3ω
Cu K-shell spectra indicate that line emission depends on laser deposition conditions → HE energy & population

Suprathermal electron temperature (fraction) scaling at moderate laser intensities:
$T_{HE} = 215\times(I_{18}\lambda^2)^{1/3}$ keV
*Beg FN et al, PoP **4** (1997) 447*
$f_{HE} \approx (I_{18}\lambda^2)^{3/4}$
*Yu J et al, PoP **6** (1999) 1318*

Characteristic X-ray Emission in High-Energy-Density Systems:
Ionic resonance lines in highly ionized atoms (quasi-optical transitions)
Inner shell transitions in weakly ionized (hollow) atoms (due to HE action)

Cu K-shell Emission vs. Ionic Charge & Plasma Temperature

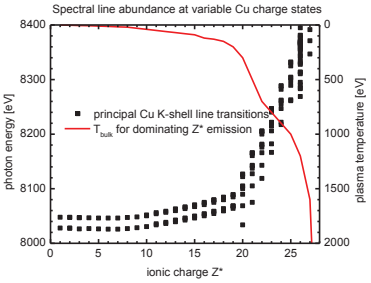

K-shell photon energy shifts with ion charge Z* for each ionic stage and given HE fraction f_{HE} emission peaks at different T_{bulk}
Spectra in ΔE range covered cannot be modelled by single T_{bulk}

FLYCHK modeling of Cu K-shell (2p → 1s) emission vs. Z*
($K\alpha_{1,2}$ line position 8047.8 and 8027.8 eV)
*Chung HK et al, HEDP **1** (2005) 3*

Effect of Hot Electron Fraction at Low and High T_{bulk}

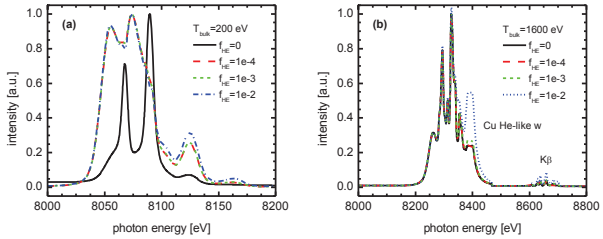

Cu K-shell emission
synthesized for ρ = 0.894 g/cm³, L = 70 μm, f_{HE} = 0, 10^{-4}, 10^{-3}, and 10^{-2}
T_{bulk} = 200 eV: code-predicted data multiplied by a **scaling factor 3×10^{12}, 90, 9, and 1, respectively**
T_{bulk} = 1600 eV: effect of HE negligible, no scaling
Calculations with $f_{HE}=1\times10^{-3}$ indicate that effect of f_{HE} on K-shell emission is dominant for **$T_{bulk}\leq800$ eV,** for higher T_{bulk} it is of secondary importance
*Šmíd M et al, Phys. Scr. **T145** (2014) 014020*

Definition of Spectral Ranges for Image Analysis

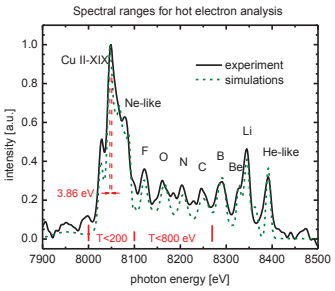

Cu K-shell emission: Experiment vs. MULTI2D modelling
Ramis R et al, Comput, Phys. Commun. 180 (2009) 977; Renner O et al, IFSA 2013
ΔE = 8 – 8.1 keV spectra characterize HE action in cold Cu (T_{bulk}<200 eV)
8 – 8.265 keV range applicable for univocal HE analysis
above 8.265 keV (T_{bulk} > 800 eV), effect of f_{HE} is ambiguous

K-shell Spectra Supported Interpretation of 2D Imaging

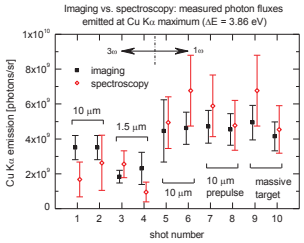

Quantitative interpretation of 2D monochromatic images
i) Cu Kα signal above background → source emission in ΔE_i=3.86 eV
ii) correction for full K-shell fluorescence (factor F)
iii) relation of photon fluxes to HE population

i) Ray-tracing calculations relate 1 photon recorded by imaging to **5.2×10^5** photons emitted from the source to 4π; for spectroscopy we get **4.4×10^7** photons
ii) Finding integrated intensity ratios between ΔE_i=3.86 eV and ΔE_s=265 eV
iii) Photons dn_K generated by 1 HE with energy E_0 and emitted in 1 sr at angle ψ

$$dn_K = \sigma_K(E)\, n_{Cu} W_K dx, \qquad dn_\psi = dn_K \frac{d\Omega}{4\pi} exp\left(-\frac{x}{l_a sin\psi}\right), \quad \text{where}$$

σ is collisional cross-section, n_{Cu} Cu atom density, W_k probability of radiative Kα deexcitation, x distance from surface and l_a characteristic Kα absorption length
*Podorov SG et al, JPD **34** (2001) 2363; Kostenko OF et al, Quant. El. **43** (2013) 237*

Penelope Code Modelling of HE Deposition in Massive Cu

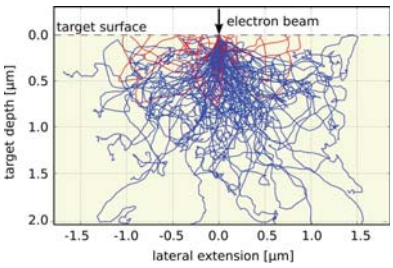

Simulation of electron collisions, generation and transport of x-rays
performed using the Monte Carlo code PENELOPE (E_0 = 30 keV)
Salvat F et al, OECD NEA (2009) 6416
3D trajectories of HE inside the target: most energy deposited within ~1.5 μm,
although Continuous-Slowing-Down-Approximation predicts ~8 μm
http://physics.nist.gov/PhysRefData /Star/Text/ESTAR.html

Penelope Predicted Cu Kα Emission

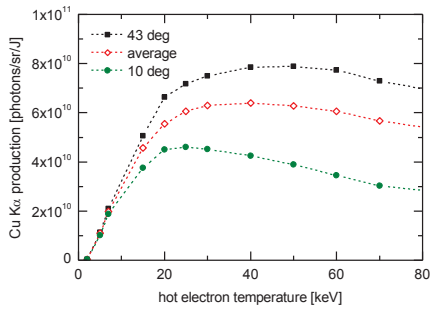

***T_{HE}*- dependent photon fluxes for 1J dose of Maxwellian-distributed HE**
shown observation angles correspond to line of sight of spectrometer (10°), imaging (43°), and average emission above the irradiated target surface

Photon Fluxes Reconstructed from X-ray Images

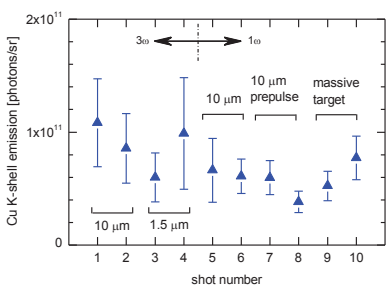

Measured photon fluxes corrected with respect to Cu Kα emission
in imaging range ΔE_i=3.86 eV and spectral range ΔE_s=265 eV
Experimentally determined average values of corrective factor *F*
13.1 for 1ω and 32.7 for 3ω laser radiation

Conversion Efficiency of Laser Energy into Hot Electrons

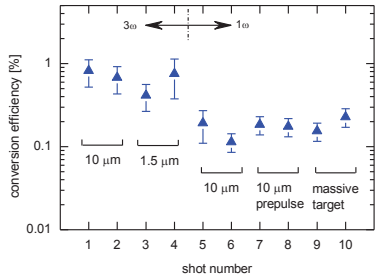

Conditions of laser energy deposition modified
using 1ω and 3ω radiation, variable Cu thickness & plasma scale length
Found conversion efficiencies 0.11-0.23% (1ω) and 0.4-0.8% (3ω)
comparable with previous observation of HE generation at coated targets
*Yu J et al, PoP **19** (2012) 012704*

Details on HE Production at 1.5-μm-thick Cu foil

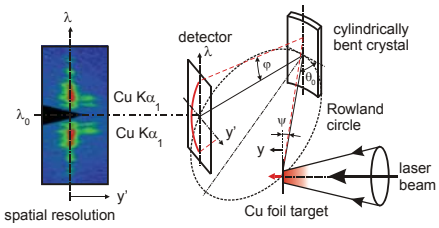

High-dispersion 1D spatially resolved Cu Kα-group spectra
recorded using vertical-geometry Johann spectrometer
*Renner O. et al, RSI **68** (1997) 2393*
Characteristics: ψ= 0 ± 0.8°, quartz (400), R = 76.6 mm, film detection spectral resolution >8 000, spatial 5.3 μm, D_{linear} ~830 mm/Å, Δλ=2×50 mÅ collection efficiency 10^2 higher than flat crystal

Spatially Resolved Information on Hot Electron Deposition

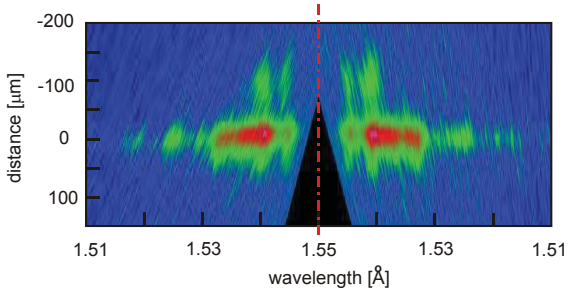

Detailed spatially resolved Cu K-shell spectra
indicate deposition of suprathermal electrons in near-surface plasma and in the phase of expanding foil stagnation
Experimental data consistent with **RALEF2D Code Modeling** confirming existence of quasi-solid density matter in relatively cold deflected foil
*Basko MM, J. Comp. Phys. **228** (2009) 2175; Šmíd M et al, to be published*

Conclusions

- **High-resolution x-ray spectroscopy provides an efficient tool for studies of hot dense laser-produced plasmas**
- **K-shell imaging is relatively simple, high-collection efficiency, and easy-to-implement method for monitoring hot electron generation and propagation inside targets**
- **Combination of imaging with high resolution x-ray spectroscopy provides a novel approach to quantitative characterization of suprathermal electrons in shock-ignition-relevant plasmas**